



PCCP

**CO<sub>2</sub> Coverage on Pd Catalysts Accelerates Oxygen Removal  
in Oxy-Combustion Systems**

Journal:	<i>Physical Chemistry Chemical Physics</i>
Manuscript ID	CP-ART-10-2022-004788.R1
Article Type:	Paper
Date Submitted by the Author:	17-Jan-2023
Complete List of Authors:	Jung, Sungyoon; Washington University in St Louis, Energy, Environmental and Chemical Engineering Cao, Tengfei; Washington University in St Louis, Mechanical Engineering and Materials Science Mishra, Rohan; Washington University in St Louis, Mechanical Engineering and Materials Science Biswas, Pratim; University of Miami College of Engineering, Chemical, Environmental and Materials Engineering

SCHOLARONE™  
Manuscripts

## ARTICLE

## CO<sub>2</sub> Coverage on Pd Catalysts Accelerates Oxygen Removal in Oxy-Combustion Systems

Sungyoon Jung<sup>a</sup>, Tengfei Cao<sup>b</sup>, Rohan Mishra<sup>b</sup>, and Pratim Biswas<sup>\*a,c</sup>Received 00th January 20xx,  
Accepted 00th January 20xx

DOI: 10.1039/x0xx00000x

Oxy-combustion systems result in enriched CO<sub>2</sub> in the exhaust gases; however, the utilization of the concentrated CO<sub>2</sub> stream from oxy-combustion is limited by remnant O<sub>2</sub>. CH<sub>4</sub> oxidation using Pd catalysts has been found to have a high O<sub>2</sub>-removal efficiency. Here, the effect of the excess CO<sub>2</sub> in the feed stream on O<sub>2</sub> removal with CH<sub>4</sub> oxidation is investigated by combining experimental and theoretical approaches. Experimental results reveal complete CH<sub>4</sub> oxidation without any side-products, and a monotonic increase in the rate of CO<sub>2</sub> generation with increase in CO<sub>2</sub> concentration in the feed stream. Density-functional theory calculations show that high surface coverage of CO<sub>2</sub> on Pd leads to a reduction in the activation energy for the initial dissociation of CH<sub>4</sub> into CH<sub>3</sub> and H, and also the subsequent oxidation reactions. A CO<sub>2</sub>-rich environment in oxy-combustion systems is therefore beneficial for the reduction of oxygen in the exhaust gas.

### Introduction

Oxy-combustion systems using enriched O<sub>2</sub> in the feed stream are effective for producing enriched CO<sub>2</sub> in the exhaust gases from power plants.<sup>1-4</sup> A concentrated CO<sub>2</sub> stream (>63%) in the exhaust gas can be obtained from oxy-combustion systems and can be further utilized for enhanced oil recovery (EOR),<sup>5</sup> conversion to useful products,<sup>6, 7</sup> or sequestration<sup>8</sup>. However, its applications are hampered by high remnant O<sub>2</sub> concentrations (~3%) that can cause corrosion inside transport pipes.<sup>9, 10</sup> The United States Department of Energy has set the targeted maximum concentration of O<sub>2</sub> to 100 parts per million volume (ppmv) for EOR.<sup>9</sup> This requires efficient strategies to reduce the O<sub>2</sub> concentration in the exhaust gas stream of oxy-combustion systems.

Catalytic CH<sub>4</sub> oxidation has been designed to remove O<sub>2</sub> from the CO<sub>2</sub> stream. Recent studies have shown their positive progress towards effective O<sub>2</sub> removal.<sup>11-13</sup> Supported catalysts using noble metals (e.g., Pd and Pt) and non-noble metals (e.g., Cu) have shown a high removal efficiency of O<sub>2</sub> (>95%) at relatively low temperatures (<773 K).<sup>11-13</sup> The gas composition in the feed stream has been reported to have a significant consequence on the reactions involving O<sub>2</sub>. Kuhn *et al.*<sup>12</sup> reported that under O<sub>2</sub>-rich or near stoichiometric conditions (O<sub>2</sub>/CH<sub>4</sub> = 2) in the feed stream, complete CH<sub>4</sub> oxidation was the major reaction. However, under O<sub>2</sub>-poor conditions, CO is also generated via dry reforming of CH<sub>4</sub>. Even though CO<sub>2</sub> is the dominant component in the feed stream, there are

only a handful of reports on the effect of excessive CO<sub>2</sub> on O<sub>2</sub> removal and CH<sub>4</sub> oxidation. A recent study reported a linear correlation between the concentration of CO<sub>2</sub> in the feed stream and the conversion rate of O<sub>2</sub> under slightly O<sub>2</sub>-rich conditions (O<sub>2</sub>/CH<sub>4</sub> ≈ 2.3).<sup>14</sup> Increased efficiency of O<sub>2</sub> removal via complete CH<sub>4</sub> oxidation was observed with an increase in CO<sub>2</sub> concentration in the feed stream. However, the underlying mechanisms for these observations are not clear. According to reported studies, a positive correlation between the concentration of the initial component and the reaction rate could be attributed to two different effects, namely the autocatalytic effect and the surface-coverage effect.<sup>15, 16, 17, 18, 19</sup> Autocatalytic effect, i.e., self-replication, defines a reaction in which the product acts as a catalyst.<sup>15</sup> It has been widely applied in various applications such as methanol synthesis in the presence of water<sup>16</sup> and the reaction of CO with OH radical to form CO<sub>2</sub> (CO+OH•→CO<sub>2</sub>+H•) in the presence of supercritical CO<sub>2</sub>.<sup>17</sup> In these reactions, the accelerated reaction rate is enabled by a reduction in the activation energy barriers through the creation of new intermediates from the products.<sup>16, 17</sup> The coverage effect could also result in an accelerated reaction rate; however, the product is not involved in the reaction as a catalyst. Instead of directly participating in the reaction, it covers the surface and decreases the activation energy barrier by modifying the surface electronic structure.<sup>18, 19</sup> Currently, there is no clear evidence on which of these two effects result in the accelerated reaction rate of O<sub>2</sub> and CH<sub>4</sub> oxidation as observed in the experiments.

In this study, the effect of excess CO<sub>2</sub> in the feed stream on the complete CH<sub>4</sub> oxidation reaction was investigated using a combination of experiments and theoretical calculations. Pd-TiO<sub>2</sub> nanoparticle catalysts were synthesized and were used to examine the effect of excess CO<sub>2</sub> in the feed stream on O<sub>2</sub> removal. Four different CO<sub>2</sub> concentrations in the feed stream were studied. Density-functional theory (DFT) calculations were used to understand the mechanisms of excess CO<sub>2</sub> on O<sub>2</sub> removal. Both surface coverage and autocatalytic effects were

<sup>a</sup> Department of Energy, Environmental and Chemical Engineering, Washington University in St. Louis, St. Louis, MO 63130, USA

<sup>b</sup> Department of Mechanical Engineering and Materials Science, and Institute of Materials Science and Engineering, Washington University in St. Louis, St. Louis, MO 63130, USA

<sup>c</sup> Department of Chemical, Environmental and Materials Engineering, University of Miami, Coral Gables, FL 33146, USA. E-mail: pbiswas@miami.edu

†Electronic Supplementary Information (ESI) available:

See DOI: 10.1039/x0xx00000x

examined by changing CO<sub>2</sub> coverage and by analysing their effect on the formation of new intermediates via CO<sub>2</sub>-involved side reactions. Our experiments show CH<sub>4</sub> oxidation as the primary reaction. Further, the generation rate of CO<sub>2</sub> is accelerated with an increase in the CO<sub>2</sub> concentration in the feed stream. DFT calculations on Pd (111) surface show that the surface CO<sub>2</sub> coverage determines the rate-limiting step of the CH<sub>4</sub> oxidation reaction, and increased surface coverage of CO<sub>2</sub> reduces the barriers for CH<sub>4</sub> dissociation.

## Materials and methods

Materials preparation, characterization, and experimental procedure are described first, followed by computational details.

### Synthesis of catalysts with a flame aerosol reactor (FLAR)

Pd-TiO<sub>2</sub> catalyst was synthesized by using a flame aerosol reactor (FLAR). Detailed information of the synthesis procedure is elucidated elsewhere.<sup>14</sup> Briefly, a bubbler was used to introduce titanium tetraisopropoxide (TTIP, 99.7%, Sigma-Aldrich) precursor vapor into FLAR. Appropriate amount of palladium acetylacetonate (Pd(acac)<sub>2</sub>, 97%, Sigma-Aldrich) was dissolved in xylene (reagent grade, Sigma-Aldrich) and acetonitrile (99.8%, Sigma-Aldrich) mixture (2:1, v/v) to prepare 1.3 M of the precursor solution. The mixed precursor solution was introduced into FLAR via a Collision nebulizer with N<sub>2</sub> carrier gas. Both precursors (TTIP and palladium acetylacetonate) were introduced into FLAR through the center port of the reactor. CH<sub>4</sub> and O<sub>2</sub> were introduced into FLAR through the second and the third ports of the reactor with flow rates of 0.35 L min<sup>-1</sup> and 2.5 L min<sup>-1</sup>, respectively. A flame was created via an ignition. Pd-doped TiO<sub>2</sub> nanoparticles were then created in the flame.<sup>20</sup> The produced nanoparticles were collected at the end of the system on an isopore membrane filter. The weight percent of Pd on TiO<sub>2</sub> catalyst was confirmed as ~0.76 wt% by inductively coupled plasma mass spectrometry (ICP-MS, Elan DRC ii, PerkinElmer).

The structural properties of the synthesized catalyst were determined using different analytical tools. The morphology and size of the synthesized Pd-TiO<sub>2</sub> catalyst was evaluated by scanning transmission electron microscopy (STEM) (JEOL 2100F). The oxidation state of Pd on TiO<sub>2</sub> surface was determined by X-ray photoelectron spectroscopy (XPS, Versa probe ii, Physical Electronics). XPS analysis was performed in triplicate and many spots were investigated for STEM analysis to generate representative data.

Detailed experimental setup and procedure for the catalysis experiments are provided elsewhere.<sup>14</sup> Briefly, 10 mg of the synthesized catalyst was put into a fixed bed reactor. The experiments were performed under a stoichiometric gas composition (O<sub>2</sub>/CH<sub>4</sub> = 2), and the concentration of CO<sub>2</sub> in the feed stream was varied from 0 mol m<sup>-3</sup> (0%) – 38.6 mol m<sup>-3</sup> (95.5%). The concentration of CH<sub>4</sub> in the feed stream was fixed at ~1.5%. Helium gas was used as the balance of the gas, if needed. By controlling the concentration of CO<sub>2</sub> in the feed stream, the effect of excessive amount of CO<sub>2</sub> on O<sub>2</sub> removal was investigated. Atmospheric pressure and temperatures ranging from room temperature to 773 K were applied. A total flow rate of ~3 ml min<sup>-1</sup> was controlled by using a mass-flow

controller. The initial, intermediate, and final gas compositions during the O<sub>2</sub> removal via CH<sub>4</sub> oxidation reaction were measured by gas chromatography (GC, 7890B, Agilent Technologies, Inc.) equipped with a porous layer open tubular (PLOT) capillary column and a thermal conductivity detector (TCD). Helium was used as a carrier gas.

### Computational details

DFT calculations were performed using the Vienna Ab initio Simulation Package (VASP).<sup>21</sup> The energy cut-off for the plane waves was set to 450 eV.  $1 \times 10^{-6}$  eV was the threshold of energy convergence of the self-consistent loops. During the structure optimization, the convergence criteria for forces on ions was 0.01 eV Å<sup>-1</sup>. We used projector augmented-wave (PAW) potentials<sup>22</sup> and the generalized gradient approximation (GGA) within the Perdew-Burke-Ernzerhof (PBE)<sup>23</sup> parameterization to describe the electron-ion and the electronic exchange-correlation interactions, respectively. The Brillouin zone was sampled with 3×3×1 *k*-points mesh using the Monkhorst-Pack scheme.<sup>24</sup> DFT-D3 method with Becke-Jonson damping<sup>25</sup> was used to include Van der Waals interactions between adsorbates and the slab surface. Previous studies<sup>14, 26, 27</sup> have shown that metallic Pd and/or reduced Pd oxides play a major role in the removal of O<sub>2</sub> via CH<sub>4</sub> oxidation reaction. Therefore, metallic Pd was used in our calculations. For a face-centered cubic (fcc) metal, its (111) surface has the lowest energy, followed by (100) and (110) surfaces,<sup>28</sup> which implies that (111) facets could be major surfaces of the nanoparticles. Therefore, Pd (111) was used in this study. A slab of (3 × 3) Pd (111) surface with three layers thickness and 15 Å of vacuum, as shown in Fig S1†, was created. The atoms in the bottom layer of the slab were fixed to their bulk coordinates and other layers were fully optimized. The adsorption and reactions were carried out on the created Pd (111) surface. Number (*n*) of adsorbate molecules on the surface corresponds to a coverage of *n*/9 ML (monolayer). For example, one adsorbate molecule on the surface indicates a coverage of 0.11 (1/9) ML.

The adsorption energy  $E_{ads}$  (eV) of molecules is defined as:

$$E_{ads} = E_{adsorbate/slab} - (E_{adsorbate} + E_{slab}), \quad (1)$$

where  $E_{adsorbate/slab}$ ,  $E_{adsorbate}$ , and  $E_{slab}$  represent the energy of the adsorbed system, the molecule in the gas phase, and the slab, respectively. A negative adsorption energy indicates that the adsorption of molecules is an exothermic reaction, while a positive adsorption energy indicates an endothermic reaction. Four different high symmetric adsorption sites: top sites (top), bridging ones (bridge) and the hollow sites (fcc, and hcp), as shown in Fig S1†, were selected to calculate the most favorable adsorption site. The optimized structures of adsorbed molecules are shown in Fig S2†.

To investigate the transition states and the activation energies ( $E_a$ , eV), the nudged elastic-band method (NEB)<sup>29</sup> was used to identify the saddle points. 15 or 18 images between initial and final structures were created and used for NEB calculations. The highest energies and the resulting images were assigned activation energies and transition state structures. Zero-point energy (ZPE) corrections<sup>30</sup> have been calculated for select cases to determine their effect on the activation energy of CH<sub>4</sub> dissociation reaction.

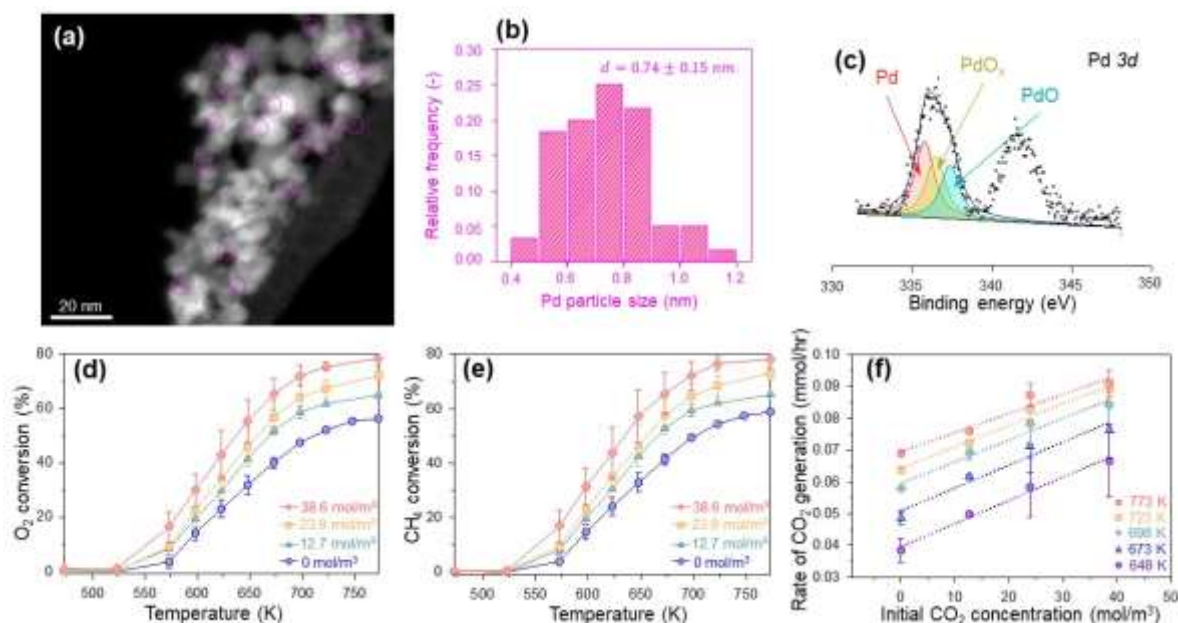


Fig 1. (a) STEM Z-contrast image of Pd-doped TiO<sub>2</sub> nanoparticles. (b) A histogram of the size distributes of Pd clusters. (c) XPS spectra of Pd, conversion of (d) O<sub>2</sub> and (e) CH<sub>4</sub> with increasing temperature and increasing concentration of CO<sub>2</sub> in the feed stream, and (f) the generation rate of CO<sub>2</sub> as a function of initial CO<sub>2</sub> concentration.

## Results and discussion

### Experimental results

#### Structure and composition of the Pd-TiO<sub>2</sub> catalysts

The morphology and the size of the synthesized Pd-TiO<sub>2</sub> nanoparticles were investigated by STEM using Z-contrast imaging. A representative image of the nanoparticles is shown in Fig 1a. In this imaging mode, heavier atoms with higher atomic number (*Z*), such as Pd, appear brighter.<sup>31</sup> The synthesized TiO<sub>2</sub> nanoparticles were observed to have a spherical shape (~8 nm). Pd clusters were found to be well-dispersed on the TiO<sub>2</sub> supports (bright dots inside pink circles in Fig 1a). The size distribution of Pd clusters was evaluated and is shown in Fig 1b. The average size of Pd clusters was determined to be 0.74 nm ± 0.15 nm.

The oxidation state of Pd was evaluated using XPS, and the corresponding spectra are shown in Fig 1c. We found that Pd existed as three different species, which were metallic Pd (335.7 eV), intermediate PdO<sub>x</sub> (0 < *x* < 1) (336.42 eV), and PdO (337.4 eV).<sup>32</sup> According to our recent study,<sup>14</sup> metallic Pd among three Pd species showed a linear dependence to the apparent reaction rate constant, which indicates that metallic Pd plays a major role for O<sub>2</sub> removal. The total surface area of metallic Pd was calculated as ~220 cm<sup>2</sup> in this study. Previous studies also show that metallic Pd plays a dominant role in O<sub>2</sub> removal and complete CH<sub>4</sub> oxidation.<sup>14, 26, 27</sup> Therefore, metallic Pd was used for further DFT calculations.

#### Effect of CO<sub>2</sub> concentration in the feed stream on O<sub>2</sub> removal

To investigate the effect of CO<sub>2</sub> in the feed stream on the O<sub>2</sub> removal via complete CH<sub>4</sub> oxidation, experiments were performed with initial CO<sub>2</sub> concentrations varying from 0 mol m<sup>-3</sup> to 38.6 mol m<sup>-3</sup>, and with helium as the balance of the gas, under stoichiometric conditions (O<sub>2</sub>/CH<sub>4</sub>=2). As can be seen in Figs 1d and 1e, both conversion rate of O<sub>2</sub> and CH<sub>4</sub> increased,

when the CO<sub>2</sub> concentration in the feed stream was increased. To clearly see the correlation between the reaction rate and the initial CO<sub>2</sub> concentration, the generation rate of CO<sub>2</sub> versus the initial CO<sub>2</sub> concentration is plotted in Fig 1f. The plot shows that the generation rate of CO<sub>2</sub> is proportional to the initial CO<sub>2</sub> concentration. The generation rate of CO<sub>2</sub> (mmol hr<sup>-1</sup>) versus the initial concentration of CO<sub>2</sub> (mol m<sup>-3</sup>) at different temperatures can be explained by a linear dependence (*R*<sup>2</sup> > 0.92). As explained in the introduction part, it can be defined as either an autocatalytic effect or a coverage effect of CO<sub>2</sub>. The accelerated reaction rate could be supported by the lower activation energy barriers via creation of new intermediates (autocatalytic effect) or via modification of the surface (surface coverage effect).<sup>16-19</sup> Based on the experimental results, it could be concluded that CO<sub>2</sub> is directly or indirectly involved in the O<sub>2</sub> removal via the complete CH<sub>4</sub> oxidation reaction. To distinguish between the autocatalytic and surface coverage effects, DFT calculations were carried out, and the corresponding results are described in the following sections. It should be noted that, we do not find the generation of H<sub>2</sub> or CO during the reaction, which implies that there is only one reaction, i.e., complete CH<sub>4</sub> oxidation. We also detect the closed values between the reaction rates of CH<sub>4</sub> and half of the reaction rate of O<sub>2</sub> (Table S1), which proves the complete CH<sub>4</sub> reaction. Thereby, the complete CH<sub>4</sub> oxidation reaction was applied for further DFT calculations.

### Computational results

#### CO<sub>2</sub> adsorption on Pd (111)

It has been demonstrated that the CO<sub>2</sub> molecule is first physisorbed and is then chemisorbed on the metal surface.<sup>28</sup> In this study, various configurations of CO<sub>2</sub> were considered and their adsorption on Pd was investigated. As depicted in Fig 2, regardless of its initial configuration, CO<sub>2</sub> molecules preferred to be weakly physisorbed on Pd (111) surface. The bond length

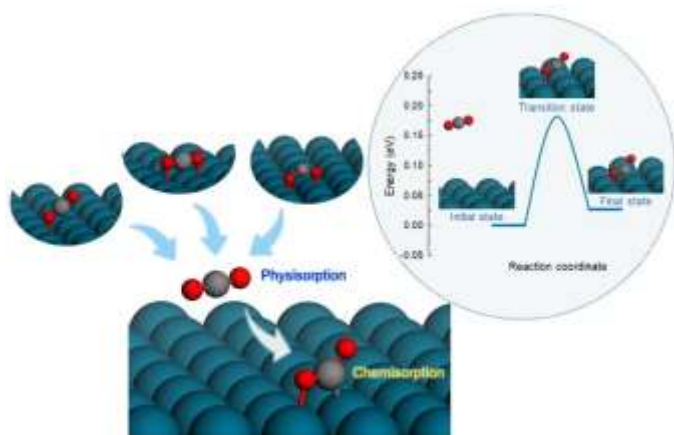


Fig 2. CO<sub>2</sub> adsorption on Pd (111). Blue, red, and grey atoms represent Pd, O, and C, respectively. Three models in the inset show the initial structures of CO<sub>2</sub>.

between C and O atoms was  $\sim 1.18$  Å and the angle of O-C-O was  $179.3^\circ$ . The distance between O atom and topmost Pd (111) surface was  $3.15$  Å. The physisorbed CO<sub>2</sub> molecule could then transform into chemisorption by forming O-Pd bonds and exist in a bidentate configuration. The lengths between C and O atoms were  $\sim 1.21$  Å and  $\sim 1.26$  Å, and the angle of O-C-O was  $138^\circ$ . The distance between O atom and topmost Pd was  $2.16$

Å. The adsorption energy of the chemisorbed CO<sub>2</sub> on Pd (111) was calculated to be  $0.03$  eV, which is similar to the previously reported value on Pd (111).<sup>33</sup> It is much lower than the reported adsorption values on non-metal surfaces such as Si- and Se-doped graphene ( $0.18$  eV and  $0.21$  eV).<sup>30</sup> It indicates that the noble metal creates a favorable environment for CO<sub>2</sub> adsorption on its surface, while CO<sub>2</sub> desorption can also easily occur with its lower CO<sub>2</sub> capture ability. The activation energy between the gaseous CO<sub>2</sub> and the chemisorbed CO<sub>2</sub> was calculated as  $\sim 0.18$  eV (Fig 2). This small activation energy barrier indicates that CO<sub>2</sub> could chemisorb on Pd (111) surface in the reaction. However, the final state of the chemisorbed CO<sub>2</sub> is slightly uphill, which implies that the reaction is a slightly endothermic reaction. Therefore, chemisorbed CO<sub>2</sub> molecules could easily desorb from Pd (111) surface. However, under our experimental condition, i.e., with excessive CO<sub>2</sub> concentration in the initial gas stream, some CO<sub>2</sub> molecules could stay on Pd (111) surface even though other CO<sub>2</sub> molecules might desorb it. In the next section, the influence of CO<sub>2</sub> coverage on Pd (111) was examined.

#### CO<sub>2</sub> coverage on Pd (111) and its effect on CH<sub>4</sub> dissociation

Experimental results demonstrate that complete CH<sub>4</sub> oxidation is the major reaction during O<sub>2</sub> removal. Therefore,

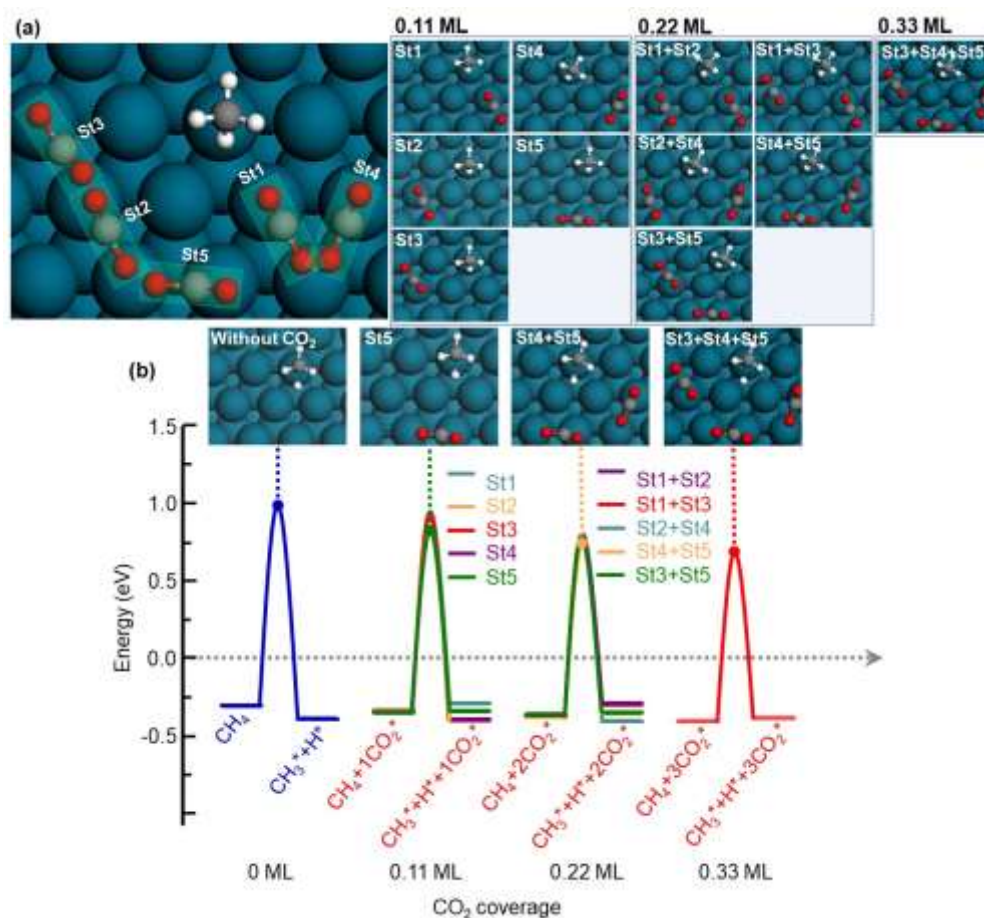


Fig 3. Coverage effect of CO<sub>2</sub> on Pd (111) surface on CH<sub>4</sub> dissociation. (a) Top view of initial configurations of CH<sub>4</sub> and CO<sub>2</sub> adsorbed on Pd (111) surface with various surface CO<sub>2</sub> coverages. (b) Energy diagrams of CH<sub>4</sub> dissociation with different surface CO<sub>2</sub> coverages and configurations. Inset shows top view of intermediates and adsorbed CO<sub>2</sub> on Pd (111) of specific surface CO<sub>2</sub> coverage showing the minimum activation energy. Blue, red, grey, and white atoms represent Pd, O, C, and H atoms, respectively.

Table 1. Reaction energies and activation energies for CH<sub>4</sub> dissociation with various surface CO<sub>2</sub> coverages.

Surface CO <sub>2</sub> coverage				Surface HOCO coverage			
Coverage (ML)	Configuration	$E_a$ (eV)	$\Delta E$ (eV)	Coverage (ML)	Configuration	$E_a$ (eV)	$\Delta E$ (eV)
0	-	1.29	-0.090	0	-	1.29	-0.090
0.11	St1	1.28	0.050	0.11	St1	1.28	-0.067
	St2	1.18	-0.055		St2	1.22	0.083
	St3	1.29	-0.064		St3	1.24	-0.048
	St4	1.17	-0.046				
	St5	1.16	0.010				
0.22	St1+St4	1.18	-0.033	0.22	St2+St3	1.12	0.181
	St1+St5	1.12	0.026		St1+St3	1.18	-0.039
	St2+St3	1.17	0.062		St1+St2	1.28	0.102
	St2+St4	1.17	0.074				
	St3+St5	1.15	0.013				
0.33	St1+St3+St5	1.10	0.021	0.33	St1+St2+St3	1.25	0.304
Average	0	1.28	-0.090	Average	0	1.28	-0.090
	0.11	1.22	-0.021		0.11	1.25	-0.010
	0.22	1.16	0.029		0.22	1.19	0.081
	0.33	1.10	0.013		0.33	1.25	0.304

further calculations were performed based on completed CH<sub>4</sub> oxidation reactions. Previously, researchers have conducted extensive mechanistic studies of complete CH<sub>4</sub> oxidation with various catalysts.<sup>34-41</sup> In those studies, reaction mechanisms and rate-limiting steps on the active catalytic surfaces under different conditions have been reported. Experimental studies revealed gaseous intermediates and products, such as CO and CO<sub>2</sub>, by using gas chromatography, and also elucidated adsorbed surface intermediates, such as formate and carbonate species, by using in-situ diffuse reflectance infrared Fourier transform spectroscopy (in situ DRIFTS) analyses, which were used to conclude possible reaction pathways.<sup>34-36</sup> Theoretical studies investigated various reaction pathways and their activation energy barriers to find the overall reaction pathways and the reaction energy landscape.<sup>37-40</sup> It is widely accepted that the dissociation of CH<sub>4</sub> is the rate-limiting step.<sup>38, 40</sup> As a first step, various CO<sub>2</sub> coverages (0.11 ML, 0.22 ML, and 0.33 ML, ML is monolayer) on Pd (111) surface were used to investigate their effect on the CH<sub>4</sub> dissociation. Since the adsorption energy of CO<sub>2</sub> is very weak (~ 0.03 eV), and it has been proved that chemisorbed CO<sub>2</sub> can easily diffuse on Pd(111) surface by crossing a low barrier,<sup>28</sup> we assume that CO<sub>2</sub> can adsorb on different sites of Pd (111) surface (Fig 3a). Depending on relative positions between CO<sub>2</sub> and CH<sub>4</sub>, we consider their different combination on Pd (111) surface for 0.22 ML and 0.33

ML, and these structures are chosen because they are most compacted on Pd (111) surface, and their surface coverage match well with experimental observations. Reaction energy ( $\Delta E$  (eV) =  $E_{Final\ state} - E_{Initial\ state}$ ) and activation energy ( $E_a$ , obtained from the saddle point energy) with and without CO<sub>2</sub> were calculated and the results are shown in Fig 3b and Table 1. We can summarize four points here: Firstly, CH<sub>4</sub> dissociation without CO<sub>2</sub> is a slightly exothermic reaction with an activation energy barrier of 1.29 eV. Secondly, regardless of different CO<sub>2</sub> coverage, the adsorption of CO<sub>2</sub> slightly reduced the energy of the initial structure (CH<sub>4</sub>+xCO<sub>2</sub>\*, x=1 or 2 or 3, \* indicates the adsorbed species), which indicates the enhanced adsorption of CH<sub>4</sub> on Pd (111) surface in the presence of CO<sub>2</sub>. For example, the energy of the initial CH<sub>4</sub> with a CO<sub>2</sub> coverage of 0.33 ML shown in Fig 3a on Pd (111) surface is ~0.1 eV lower than that without CO<sub>2</sub>. Thirdly, the activation energy of CH<sub>4</sub> dissociation with CO<sub>2</sub> was lower than that without CO<sub>2</sub>, so, CO<sub>2</sub> adsorption facilitates CH<sub>4</sub> reaction (Fig 4a). Fourthly, the activation energy of CH<sub>4</sub> dissociation was dependent on the CO<sub>2</sub> coverage. To clearly see the trend of CO<sub>2</sub> coverage and CH<sub>4</sub> dissociation, the activation energy of CH<sub>4</sub> dissociation is plotted as a function of CO<sub>2</sub> coverage on Pd (111) surface and is shown in Fig 4b. It can be observed that, as CO<sub>2</sub> coverage increases, the activation energy of CH<sub>4</sub> dissociation decreases, which implies that adsorbed CO<sub>2</sub> on Pd (111) promotes CH<sub>4</sub> dissociation and

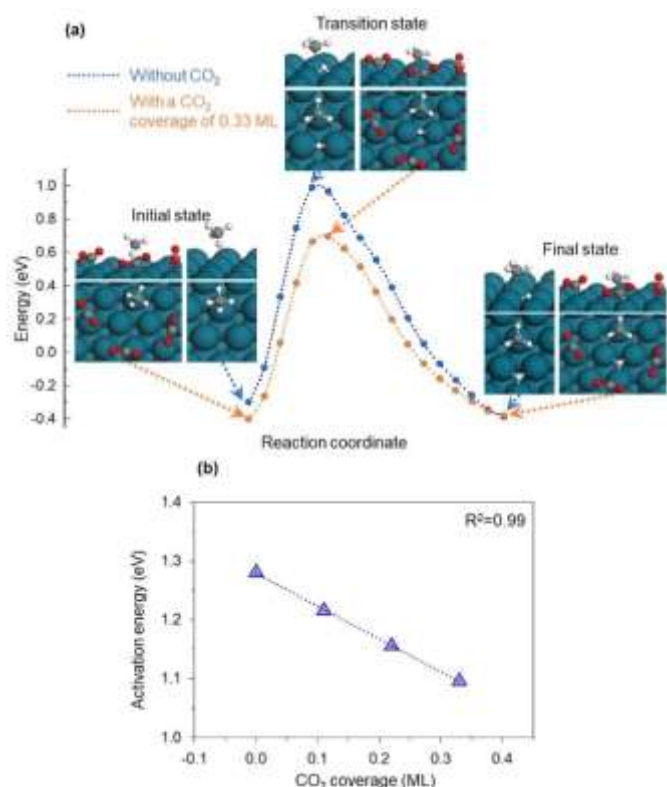


Fig 4. (a) Energy diagram of CH<sub>4</sub> dissociation without and with a CO<sub>2</sub> coverage of 0.33 ML, and (b) the variation of theoretically calculated activation energy with surface CO<sub>2</sub> coverage. Blue, red, grey, and white atoms represent Pd, O, C, and H atoms, respectively.

therefore, an increased CH<sub>4</sub> and O<sub>2</sub> conversion is expected. These results are consistent with our experimental observations (Figs 1d-f). We note that the ZPE corrections did not have any significant effect on the activation energy of CH<sub>4</sub> dissociation reaction under different surface CO<sub>2</sub> coverage (Table S2).

#### Reactions of CO<sub>2</sub> on Pd (111)

The effect of adsorbed CO<sub>2</sub> molecules and their coverage on CH<sub>4</sub> dissociation was revealed in previous section, and to fully understand our experimental detections, in this section, the possibility of other CO<sub>2</sub> reactions on Pd (111) are further investigated. The schematic diagrams of potential reactions are shown in Fig 5a: (1) direct dissociation of CO<sub>2</sub> (CO<sub>2</sub>\* → CO + O); (2) reaction between CH<sub>4</sub> and chemisorbed CO<sub>2</sub> (CO<sub>2</sub>\* + CH<sub>4</sub> → HOCO\* + CH<sub>3</sub>\*); (3) reaction with adsorbed CH<sub>3</sub> and chemisorbed CO<sub>2</sub> (CO<sub>2</sub>\* + CH<sub>3</sub>\* → COOCH<sub>3</sub>\*); (4) reaction with adsorbed H and chemisorbed CO<sub>2</sub> (CO<sub>2</sub>\* + H\* → HOCO\*) (\* indicates the adsorbed species). Reactions 3 and 4 are related to the products of CH<sub>4</sub> dissociation, i.e., CH<sub>3</sub> and H. Four different adsorption sites (Fig S1†) were considered to determine the optimized initial and final structures, and their transition states. The results are shown in Fig 5b. Most of these side reactions have high activation energies. Specifically, the reaction with CH<sub>4</sub> has the highest activation energy (~ 2.65 eV), followed by the direct dissociation of CO<sub>2</sub> (~ 2.34 eV), adsorbed CH<sub>3</sub> (~ 2.10 eV), and the reaction with adsorbed H (~ 0.97 eV). Due to their high activation energies, we propose that, apart from the reaction between adsorbed H and chemisorbed CO<sub>2</sub>, other reactions can hardly exist in our experiments. The activation energy of the reaction with adsorbed H is comparative with the reaction

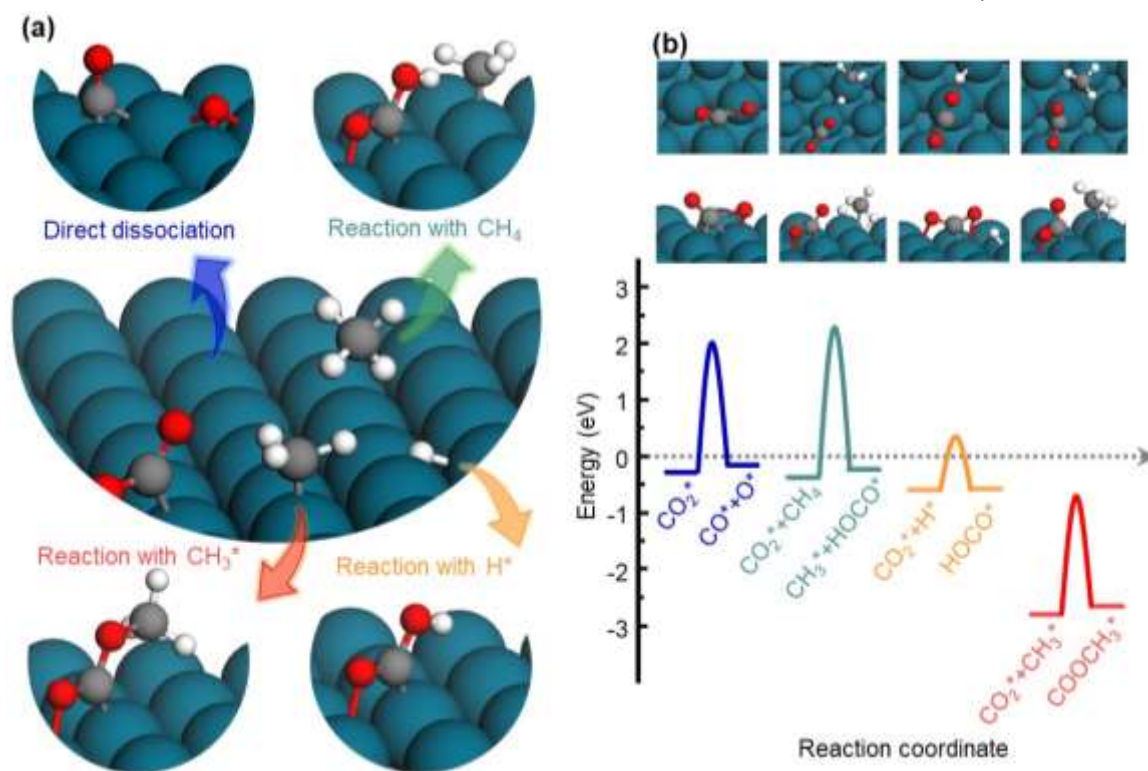


Fig 5. (a) Possible intermediates of various CO<sub>2</sub>-involved side reactions on Pd (111) surface. (b) Energy diagram for various CO<sub>2</sub>-involved reactions on the Pd (111) surface. The models at the top of the plot show the top view (top) and side view (bottom) of intermediates at the transition state. Blue, red, grey, and white atoms represent Pd, O, C, and H atoms, respectively.

between adsorbed O and adsorbed H ( $\sim 1.24$  eV) (Fig S3<sup>†</sup>), which implies that adsorbed H possibly reacts with both adsorbed O and adsorbed CO<sub>2</sub>. Therefore, the product (HOCO) from the reaction between adsorbed CO<sub>2</sub> and adsorbed H might affect the CH<sub>4</sub> dissociation as well.

#### HOCO coverage on Pd (111) and its effect on CH<sub>4</sub> dissociation

We further analyzed the effect of HOCO\* coverage (0.11 ML, 0.22 ML, and 0.33 ML, ML is monolayer) — that can be produced during CO<sub>2</sub>\*+H\*→HOCO\* reaction — on CH<sub>4</sub> dissociation. Similar to the above studied CO<sub>2</sub> coverage effects, different adsorption sites were considered (inset in Fig 6a), and different HOCO and CH<sub>4</sub> combinations for 0.22 ML and 0.33 ML were considered.  $\Delta E$  and  $E_a$  for CH<sub>4</sub> dissociation on Pd (111) with and without HOCO were calculated and the results are shown in Figs 6b and Table 1. According to the obtained results, we can conclude that, being similar to CO<sub>2</sub>, HOCO also slightly promotes CH<sub>4</sub> adsorption on Pd (111) surface. It can be observed that the energy of the initial CH<sub>4</sub> with the HOCO coverage of 0.33 ML was  $\sim 0.05$  eV lower than that without HOCO. The CH<sub>4</sub> dissociation with different HOCO coverages was mostly endothermic, i.e., higher energy at the final state compared to the initial state, and the activation energy of CH<sub>4</sub> dissociation was not strongly dependent on the adsorption site of HOCO on Pd (111). Moreover, the activation energies of CH<sub>4</sub> dissociation with HOCO coverages of 0.11 ML and 0.22 ML were

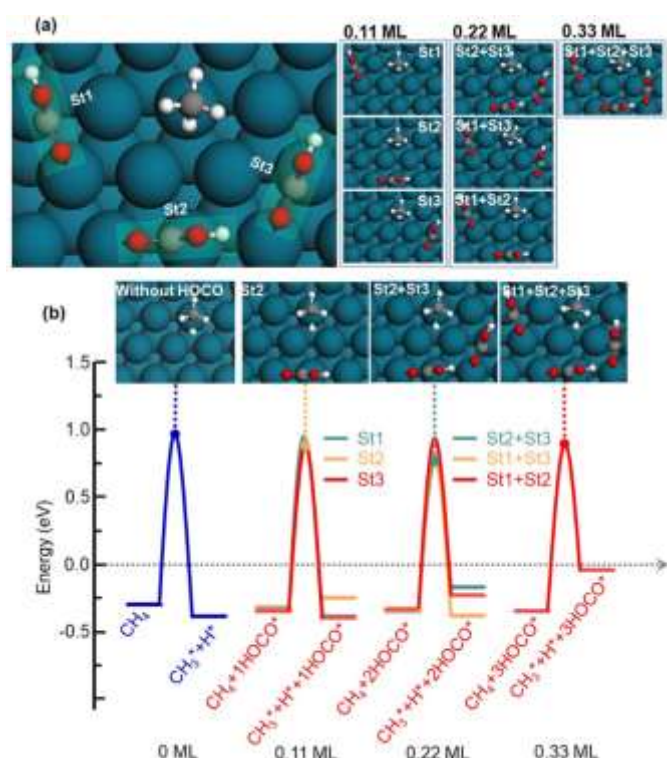


Fig 6. The effect of HOCO coverage on Pd (111) surface on CH<sub>4</sub> dissociation. (a) Top-view of initial configurations of CH<sub>4</sub> and HOCO adsorbed on a Pd (111) surface with various surface HOCO coverages. (b) Energy diagrams of CH<sub>4</sub> dissociation with different surface HOCO coverages. Inset shows top view of intermediates and adsorbed HOCO on Pd (111) of specific surface HOCO coverage showing the minimum activation energy. Blue, red, grey, and white atoms represent Pd, O, C, and H atoms, respectively.

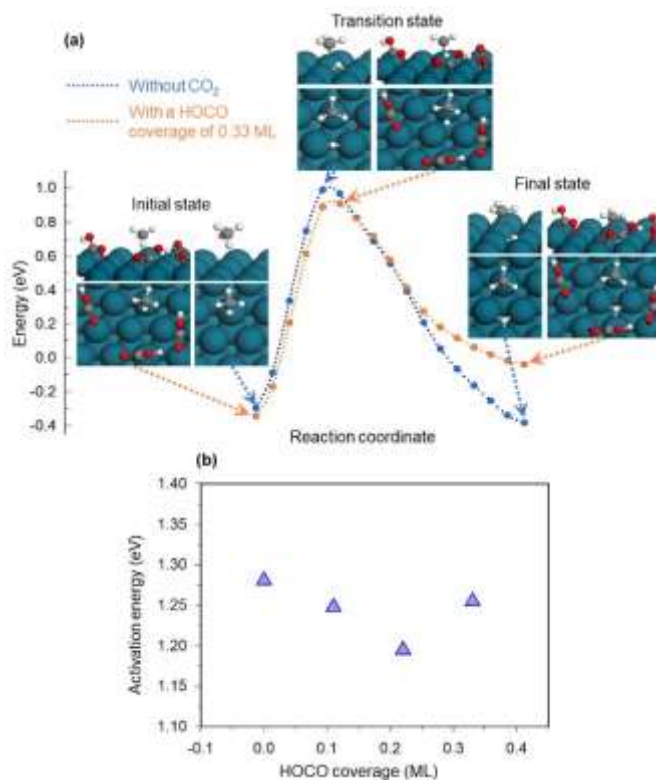


Fig 7. (a) Energy diagram of CH<sub>4</sub> dissociation without and with a HOCO coverage of 0.33 ML, and (b) the change in activation energy with increasing surface coverage of HOCO. Blue, red, grey, and white atoms represent Pd, O, C, and H atoms, respectively.

lower than that without HOCO, while under HOCO coverage of 0.33 ML, the activation energy was back to similar. These findings are clearly shown in energy diagram of CH<sub>4</sub> dissociation without HOCO and with a HOCO coverage of 0.33 ML in Fig 7a. To see the relation between HOCO coverage and CH<sub>4</sub> dissociation, the activation energy of CH<sub>4</sub> dissociation was plotted as a function of HOCO coverage (Fig 7b). It shows that the activation energy of CH<sub>4</sub> dissociation decreased with lower HOCO coverage on Pd (111) (0.11 ML and 0.22 ML). However, it increased with the highest HOCO coverage (0.33 ML), which indicates that high HOCO coverage is not favorable for CH<sub>4</sub> dissociation. Based on all these results, it can be concluded that CH<sub>4</sub> dissociation with HOCO coverage on Pd (111) surface is endothermic and has a higher activation than dissociation in the presence of CO<sub>2</sub>; therefore, the HOCO catalytic effects on CH<sub>4</sub> adsorption and reaction are less efficient than that of CO<sub>2</sub>. Similar to the case of CH<sub>4</sub> dissociation under different surface CO<sub>2</sub> coverage, the ZPE corrections did not have any significant effects on the activation energy of CH<sub>4</sub> dissociation under different surface HOCO coverage (Table S2).

#### Potential energy profile with CO<sub>2</sub> coverage

Based on above findings, CO<sub>2</sub> coverage was found to accelerate CH<sub>4</sub> oxidation by reducing energy barriers of decomposition from CH<sub>4</sub> to CH<sub>3</sub>\* and H\*. In this section, the effect of CO<sub>2</sub> coverage (0.33 ML) on overall complete CH<sub>4</sub> oxidation was investigated and the energy profile of complete CH<sub>4</sub> oxidation with CO<sub>2</sub> coverage is presented in Fig 8 and Table

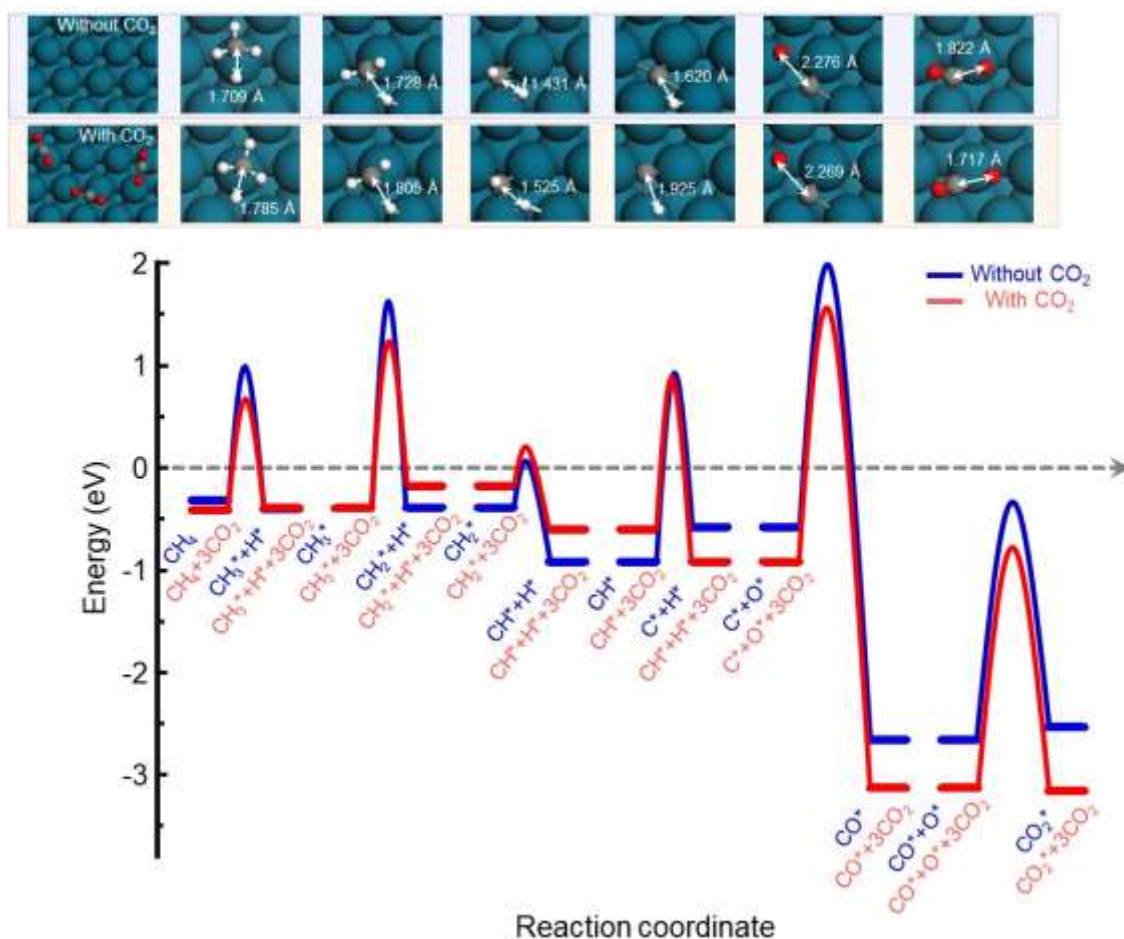


Fig 8. Energy profiles of complete CH<sub>4</sub> oxidation reaction with and without CO<sub>2</sub> coverage on Pd (111) surface. Inset shows top view of intermediates on Pd (111) surface. Blue, red, grey, and white atoms represent Pd, O, C, and H atoms, respectively.

S3. It can be found that complete CH<sub>4</sub> oxidation reaction was also sensitive to surface CO<sub>2</sub> coverage and that the activation energy is reduced by the increased surface coverage of CO<sub>2</sub>. For example, lower activation energy barriers were distinct in the dissociation process of CH<sub>3</sub> into CH<sub>2</sub> and H (1.73 eV without surface CO<sub>2</sub> coverage vs. 1.64 eV with surface CO<sub>2</sub> coverage), and that in the dissociation of CH into C and H (1.86 eV without surface CO<sub>2</sub> coverage vs. 1.48 eV with surface CO<sub>2</sub> coverage). Transition states of all reactions without surface CO<sub>2</sub> coverage are presented in the blue region in the inset in Fig 8, and those with surface CO<sub>2</sub> coverage are depicted in the red region inset of Fig 8. As can be seen in Fig 8, the distances between C and dissociated H were extended with surface CO<sub>2</sub> coverage during CH<sub>4</sub> dissociation (CH<sub>4</sub>\* → CH<sub>3</sub>\*+H\*), CH<sub>3</sub> dissociation (CH<sub>3</sub>\* → CH<sub>2</sub>\*+H\*), CH<sub>2</sub> dissociation (CH<sub>2</sub>\* → CH\*+H\*), and CH dissociation (CH\* → C\*+H\*). For example, the distance between C and dissociated H from CH<sub>3</sub> was 1.805 Å with surface CO<sub>2</sub> coverage, which is longer than 1.728 Å without surface CO<sub>2</sub> coverage. On the other hand, the distances between C and reacted O were shortened under surface CO<sub>2</sub> coverage during CO formation (C\*+O\* → CO\*) and CO<sub>2</sub> formation (CO\*+O\* → CO<sub>2</sub>\*). For instance, the distance between C and reacted O in the reaction of CO<sub>2</sub> formation was 1.717 Å with surface CO<sub>2</sub> coverage, while it was 1.822 Å without surface CO<sub>2</sub> coverage. This modified structure might be attributed to the variation of charge density

distribution under different surface CO<sub>2</sub> coverage and is consistent with result of Wu *et al.*,<sup>18</sup> which reports a charge transfer due to the modification of the charge density with surface HOCO coverage.

## Conclusions

The effect of the excessive amount of CO<sub>2</sub> in the feed stream on O<sub>2</sub> removal with CH<sub>4</sub> oxidation was investigated by combining experimental and theoretical approaches. All reactions on the surface of Pd-TiO<sub>2</sub> catalyst synthesized via an aerosol route, are experimentally studied. Experimental results revealed that there was only one major CH<sub>4</sub> oxidation reaction, and the increase of the CO<sub>2</sub> concentration in the feed stream accelerates the generation rate of CO<sub>2</sub>. DFT calculations on Pd (111) surface show that the surface CO<sub>2</sub> coverage determines the rate-limiting step of the complete CH<sub>4</sub> oxidation reaction, and the increased surface CO<sub>2</sub> coverage reduces the barriers of CH<sub>4</sub> dissociation. The CO<sub>2</sub>-containing intermediates (COOCH<sub>3</sub> and CO) are predicted to be not feasible because of their high activation energy barriers, and high coverage of HOCO inhibits the dissociation of CH<sub>4</sub> on Pd surface. Calculations of the energetics of the complete CH<sub>4</sub> reaction process show that CO<sub>2</sub> coverage accelerates complete CH<sub>4</sub> oxidation by lowering the activation energy barriers of several intermediates. All these findings emphasize the important role of CO<sub>2</sub> on the purification

process of remnant O<sub>2</sub> in the flue gas via complete CH<sub>4</sub> oxidation reaction from the oxy-combustion system. It provides a new positive aspect of the oxy-combustion system for purification of flue gas from the system due to the CO<sub>2</sub>-rich environment in it.

## Conflicts of interest

There are no conflicts to declare.

## Acknowledgements

This work was supported by a grant funded by the U.S. Department of Energy's National Energy Technology Laboratory under Award Number DE-FE0029161. R.M. acknowledges support from the National Science Foundation (NSF) through grants CBET-1729787, DMR-1931610 and DMR-1806147. This work used computational resources through allocation DMR160007 from the Extreme Science and Engineering Discovery Environment (XSEDE), which was supported by NSF ACI-1548562.

## Supplementary material

Structure of Pd (111) and its adsorption sites, optimized structures of adsorbed molecules, activation energy by image optimization, NEB, and CI-NEB, reaction rates of CH<sub>4</sub>, 1/2O<sub>2</sub>, and 1/2CO with different conditions, OH formation on Pd (111), and reaction and activation energies for elementary reaction steps on Pd (111).

## References

- B. J. P. Buhre, L. K. Elliott, C. D. Sheng, R. P. Gupta and T. F. Wall, *Prog Energy Combust*, 2005, **31**, 283-307.
- A. Gopan, B. M. Kumfer, J. Phillips, D. Thimsen, R. Smith and R. L. Axelbaum, *Appl Energy*, 2014, **125**, 179-188.
- K. Jordal, M. Anheden, J. Yan, L. Strömberg, *Greenhouse Gas Control Technologies*, 2005, **7**, 201-209.
- M. Kanniche, R. Gros-Bonnivard, P. Jaud, J. Valle-Marcos, J. M. Amann and C. Bouallou, *Appl Therm Eng*, 2010, **30**, 53-62.
- Z. X. Dai, R. Middleton, H. Viswanathan, J. Fessenden-Rahn, J. Bauman, R. Pawar, S. Y. Lee and B. McPherson, *Environ Sci Tech Let*, 2014, **1**, 49-54.
- W. N. Wang, W. J. An, B. Ramalingam, S. Mukherjee, D. M. Niedzwiedzki, S. Gangopadhyay and P. Biswas, *J Am Chem Soc*, 2012, **134**, 11276-11281.
- A. Dwivedi, R. Gudi and P. Biswas, *J CO<sub>2</sub> Util*, 2018, **24**, 376-385.
- S. Chu, *Science*, 2009, **325**, 1599-1599.
- M. Woods and M. Matuszewski, *Quality guidelines for energy system studies: CO<sub>2</sub> impurity design parameters*, NETL/DOE-341/011212; National Energy Technology Laboratory (NETL): Pittsburgh, PA, 2012.
- F. Ortloff, J. Bohnau, F. Graf and T. Kolb, *Appl Catal B-Environ*, 2016, **182**, 375-384.
- Q. H. Zheng, S. J. Zhou, M. Lail and K. Amato, *Ind Eng Chem Res*, 2018, **57**, 1954-1960.
- A. N. Kuhn, Z. Chen, Y. Lu and H. Yang, *Energy Technol-Ger*, 2019, **7**, 1800917.
- A. N. Kuhn, Y. L. Ma, C. Zhang, Z. T. Chen, M. Y. Liu, Y. Q. Lu and H. Yang, *Energy Technol-Ger*, 2020, **8**, 1901213.
- S. Jung, N. Reed, G. Yablonsky and P. Biswas, *Catal Sci Technol*, 2021, **11**, 4763-4775.
- A. J. Bissette and S. P. Fletcher, *Angew Chem Int Edit*, 2013, **52**, 12800-12826.
- Y. Yang, C. A. Mims, D. H. Mei, C. H. F. Peden and C. T. Campbell, *J Catal*, 2013, **298**, 10-17.
- A. E. Masunov, E. Wait and S. S. Vasu, *J Phys Chem A*, 2016, **120**, 6023-6028.
- P. P. Wu and B. Yang, *ACS Catal*, 2017, **7**, 7187-7195.
- K. R. Hahn, M. Iannuzzi, A. P. Seitsonen and J. Hutter, *J Phys Chem C*, 2013, **117**, 1701-1711.
- V. Tiwari, J. Jiang, V. Sethi and P. Biswas, *Appl Catal A-General*, 2008, **345**, 241-246.
- G. Kresse and J. Furthmuller, *Phys Rev B*, 1996, **54**, 11169-11186.
- P. E. Blöchl, *Phys Rev B*, 1994, **50**, 17953.
- J. P. Perdew, K. Burke and M. Ernzerhof, *Phys Rev Lett*, 1996, **77**, 3865-3868.
- H. J. Monkhorst and J. D. Pack, *Phys Rev B*, 1976, **13**, 5188.
- S. Grimme, S. Ehrlich and L. Goerigk, *J Comput Chem*, 2011, **32**, 1456-1465.
- S. W. Yang, A. Maroto-Valiente, M. Benito-Gonzalez, I. Rodriguez-Ramos and A. Guerrero-Ruiz, *Appl Catal B-Environ*, 2000, **28**, 223-233.
- K. Murata, D. Kosuge, J. Ohyama, Y. Mahara, Y. Yamamoto, S. Arai and A. Satsuma, *ACS Catal*, 2019, **10**, 1381-1387.
- L. S. Xuejing Liu, Wei-Qiao Deng, *J Phys Chem C*, 2018, **122**, 8306-8314.
- H. Jónsson, G. Mills and K. W. Jacobsen, 1998, 385-404.
- R. Gholizadeh and Y.-X. Yu, *Appl Surf Sci*, 2015, **357**, 1187-1195.
- S. Pennycook and D. Jesson, *Ultramicroscopy*, 1991, **37**, 14-38.
- F. Niu, S. Q. Li, Y. C. Zong and Q. Yao, *J Phys Chem C*, 2014, **118**, 19165-19171.
- M. H. Zhang, Y. F. Wu, M. B. Dou and Y. Z. Yu, *Catal Lett*, 2018, **148**, 2935-2944.
- O. Demoulin, M. Navez and P. Ruiz, *Appl Catal A-General*, 2005, **295**, 59-70.
- M. Schmal, M. M. V. M. Souza, V. V. Alegre, M. A. P. da Silva, D. V. Cesar and C. A. C. Perez, *Catal Today*, 2006, **118**, 392-401.
- P. Gelin and M. Primet, *Applied Catalysis B-Environmental*, 2002, **39**, 1-37.
- A. Trincherro, A. Hellman and H. Gronbeck, *Surf Sci*, 2013, **616**, 206-213.
- A. D. Mayernick and M. J. Janik, *J Catal*, 2011, **278**, 16-25.
- J. S. Yoo, J. Schumann, F. Studt, F. Abild-Pedersen and J. K. Nørskov, *J Phys Chem C*, 2018, **122**, 16023-16032.
- M. Jorgensen and H. Gronbeck, *ACS Catal*, 2016, **6**, 6730-6738.
- Y. H. (Cathy) Chin, C. Buda, M. Neurock and E. Iglesia, *J Am Chem Soc*, 2011, **133**, 15958-15978.